Published in final edited form as:
J Neurosci. 2011 July 6; 31(27): 9895–9904. doi:10.1523/JNEUROSCI.6223-10.2011.

The Striatum is Highly Susceptible to Mitochondrial Oxidative Phosphorylation Dysfunctions

Alicia M. Pickrell[1], **Hirokazu Fukui**[1,2], **Xiao Wang**[3], **Milena Pinto**[4], and **Carlos T. Moraes**[1,3,4,*]

[1]Neuroscience Graduate Program, University of Miami: Miller School of Medicine

[3]Graduate Program in Cancer Biology, University of Miami: Miller School of Medicine

[4]Department of Neurology, University of Miami: Miller School of Medicine

Abstract

Neuronal oxidative phosphorylation (OXPHOS) deficiency has been associated with a variety of neurodegenerative diseases, including Parkinson's disease and Huntington's disease. However, it is not clear how mitochondrial dysfunction alone can lead to a preferential elimination of certain neuronal populations *in vivo*. We compared different types of neuronal populations undergoing the same OXPHOS deficiency to determine their relative susceptibility and mechanisms responsible for selective neuron vulnerability.

We used a mouse model expressing a mitochondria-targeted restriction enzyme, PstI or mito-PstI. The expression of mito-PstI induces double-strand breaks in the mitochondrial DNA (mtDNA), leading to OXPHOS-deficiency, mostly due to mtDNA depletion. We targeted mito-PstI expression to the cortex, hippocampus, and striatum under the CamKII-α promoter. Animals undergoing long-term expression of mito-PstI displayed a selective worsening of the striatum over cortical and hippocampal areas. Mito-PstI expression and mtDNA depletion, were not worse in the striatum, but yet the latter showed the most severe defects in mitochondrial membrane potential, response to calcium, and survival.

These results showed that the striatum is particularly sensitive to defects in OXPHOS possibly due to an increased reliance on OXPHOS function in this area and differences in response to physiological stimuli. These results may help explain the neuropathological features associated with Huntington's disease, which have been associated with OXPHOS defects.

Keywords

neurodegeneration; mitochondria; striatum; oxidative phosphorylation

Introduction

Neurodegenerative diseases encompass an age-related regional and selective loss of specific neural cell populations that causes behavioral and mental decline depending on the extent and location of the cells that were lost. Mitochondrial dysfunction has now been closely associated with neurodegenerative diseases and neurodegenerative events (Pickrell and Moraes, ; Schon and Manfredi, 2003; Lin and Beal, 2006; Mattson et al., 2008).

*To whom correspondence should be addressed: 1420 NW 9th Avenue, Rm.229, Miami, FL 33133; Tel: 305-243-5858; Fax: 305-243-6955; cmoraes@med.miami.edu .
[2]Present address: CRTD – DFG Research Center for Regenerative Therapies Dresden

The authors declare no conflict of interests

These particular insults to the mitochondria have stemmed from different causes ranging from mutations in huntingtin protein, mitochondrial toxins, and stroke causing oxygen/glucose deprivation. Huntington's disease (HD) preferentially affects medium spiny, striatal neurons affecting mitochondria by inhibiting various oxidative phosphorylation (OXPHOS) complexes, stalling mitochondrial dynamics, and down-regulating mitochondria biogenesis transcription controller, peroxisome proliferator-activated receptor gamma coactivator 1-alpha (PGC-1α) (Cui et al., 2006; Fukui and Moraes, 2007; Orr et al., 2008; Wang et al., 2009). The exposure to mitochondrial toxins that inhibit complexes I and II, such as rotenone and 3-nitroproprionic acid, respectively, causes degeneration of the striatum (Guyot et al., 1997; Betarbet et al., 2000). Finally, middle cerebral artery and focal ischemia models also report a sensitivity of the striatum due to mitochondrial membrane potential alterations and decreased availability for energy sources in these experimental paradigms (Berthet et al., 2009; Lee et al., 2009).

In this study, we investigated region-specific susceptibilities to a neuronal OXPHOS deficiency and explored possible mechanisms for this preferential sensitivity *in vivo*. We used a transgenic mouse model expressing low steady-state protein levels of *PstI* endonuclease targeted to the mtDNA, mito-PstI. Mito-PstI causes double-strand breaks in the mtDNA depleting the levels of mtDNA over time. This results in a chronic OXPHOS-deficiency by reducing the availability of mtDNA encoded subunits. We report here that mice with this neuron-specific mtDNA depletion undergo severe striatal degeneration due to regionally distinct mitochondrial properties.

Methods

Animals

The generation of Mito-PstI transgenic mice was previously described (Fukui and Moraes, 2009). In brief, a mammalianized version of the bacterial *PstI* gene was positioned behind a 5′mitochondrial targeting sequence from human COX VIII (cytochrome *c* oxidase subunit VIII). The intervening sequence 8 (IVS8) was introduced between the tetracycline response element (TRE) promoter sequence and the mito-PstI coding sequence. Mice were crossed with C57BL/6J mice for colony maintenance. The nuclear background was mostly C57BL/6J (F4) for male animals used for behavioral testing, containing smaller genetic contributions from SJLF1 and CBA. Male animals for biochemical analysis were pure C57BL/6J mito-PstI (F10) animals crossed with CamKIIα-tTA animals of the same background (Jackson Laboratories).

All mice procedures were performed according to a protocol approved by the University of Miami Institutional Animal Care and Use Committee. Mice were housed in a virus-antigen-free facility at the University of Miami: Division of Veterinary Resources in a 12 hr light/dark cycle at room temperature and fed *ad libitum* with a standard rodent diet.

Western Blotting

Protein extracts were prepared from the cortical, hippocampal, striatal, and cerebellar neuroanatomical regions that were homogenized with a hand-held rotor (VWR) in phosphate-buffered saline (PBS) containing a protease inhibitor cocktail (Roche). Samples were then snap frozen in liquid nitrogen and stored in −80 °C until used. Upon use, sodium dodecyl sulfate (SDS) was added to the homogenate at the final concentration of 4%. Homogenates were then centrifuged at 14,000 × g and the supernant was collected for analysis. Proteins were quantified using Dc Protein Assay kit using Lowry HS methodology (BioRad). Proteins were run on either a 12% SDS-acrylamide gel or 4-20% SDS-polyacrylamide gradient gel (BioRad) depending on the predicted molecular weight. The gel

was blotted on Polyvinylidene Fluoride (PVDF) membrane (BioRad) or nitrocellulose (BioRad).

Membranes were blocked in 1:1 Odyssey blocking solution (LI-COR Biosciences) for 1 hour at room temperature. Primary antibodies used were anti-*Pst*I 1:1000 dilution (generated from our own laboratory), OXPHOS rodent cocktail 1:1000 (Mitosciences), α-tubulin 1: 2000 (Sigma), β-III tubulin 1:1000 (AbCam), GFAP 1:1000 (Cell Signaling), SDHA 1:1000 (Mitosciences), and actin 1:5000 (Sigma). Primary antibody was incubated overnight at 4°C. Secondary antibodies used were either infrared conjugated antibodies anti-rabbit-700/anti-mouse-800 (Rockland) at 1:3000-1:5000 concentrations. Secondary antibodies were incubated for 1 hour at room temperature. Blots with infrared secondary antibodies were visualized with Odyssey Infrared Imaging System (LI-COR Biosciences). Optical density measurements were taken by default software supplied by LI-COR on blots.

mRNA Isolation and Reverse Transcriptase PCR

Animals were deeply anesthetized using isofluorane, euthanized by cervical dislocation, and brains were quickly isolated. The isolated brains were further dissected into the cerebral cortex, hippocampus, striatum, and cerebellum, and were submerged in RNAlater (Ambion). Tissues were homogenized with a hand-held rotor homogenizer (VWR) and homogenates were run through QiaShredder columns (Qiagen). RNA was extracted from lysates using RNeasy Plus Mini Kit (Qiagen). We used 500 ng to 1 μg of RNA for a reverse-transcription reaction using the Superscript III kit (Invitrogen).

Isolation of Mitochondria

Mitochondria was isolated as previously described (Kirkinezos et al., 2005) with small modifications. Anesthetized animals were sacrificed immediately and regionally dissected brain regions were homogenized in a dounce glass homogenizer (8-10 strokes) in SEE buffer (250 mM sucrose, 10 mM Hepes pH 7.4, 0.5 mM EDTA pH 7.4, 0.5 mM EGTA) with the addition of 50 mg/ml bovine serum albumin (BSA) and protease inhibitor cocktail (Roche) before use. The homogenate was spun on a Sorvall Superspeed RC2-B centrifuge at 4 °C at 2,000 × g for 5 minutes. The supernatant was removed and spun at 12,000 × g for 8 minutes. The pellet was resuspended in SEE buffer and re-spun. A final spin of the resuspended pellet was performed in 250 mM sucrose. The final pellet was resuspended in mitochondria incubation buffer, pH 7.2 (130 mM KCl, 2 mM KH_2PO_4, 2 mM $MgCl_2$, 10 mM Hepes, and 1 mM EDTA). Proteins in the final suspension were measured using the Bradford methodology with a BSA standard curve using BioRad Protein Assay dye (BioRad).

TMRE Flow Cytometry

Thirty μg of mitochondria isolated by the above-mentioned procedure was aliquoted and spun at 15,000 × g on a bench-top centrifuge (Eppendorf 5424). The supernatant was removed, and the pellet resuspended in 75 nM of Tetramethylrhodamine, ethyl ester, perchlorate (TMRE, non-quenching mode) dye diluted in modified Ringer's media with the addition of 250 mM sucrose. Freshly prepared 20 mM of glutamic acid and 4 mM of malic acid were added to the reaction and incubated for 10 minutes at 37 °C in the dark. In some experimental groups, 2 μM CCCP or 0.3 μmol Ca^{2+} per mg of protein were also added to the final reaction. The supernatant was aspirated after centrifugation, and the pellet resuspended in 7.5 nM of TMRE dye diluted and prepared as stated above. Ten thousand events for each sample were read at Absorbance/Emissions = 488/560 nm on LSR Fortessa (BD Biosciences). All samples were treated with CCCP to determine the values of a complete loss of membrane potential.

Spectrophotometer Assays

OXPHOS assays were previously described (Barrientos, 2002). In summary, homogenates from cortex, hippocampus, striatum, and cerebellum were prepared using a hand-held rotor to homogenize tissue in PBS plus protease inhibitor cocktail (Roche) on ice. 2 mM cytochrome *c* reduced with sodium dithionite was added to homogenates in a buffer (10 mM KH_2PO_4, 1 mg/mL BSA, 120 mM lauryl maltoside). Samples were read at 550-580 nm with the slope reading taken for 2 minutes at 37°C. 240μM Potassium cyanide was used to inhibit the reaction to ensure slope was specific to COX. Readings were normalized by protein concentration determined by Bradford methodology.

Homogenates for citrate synthase were added to a buffer (50mM Tris-HCl pH 7.5, 20mM Acetyl CoA, 10mM 5,5′-dithiobis (2-nitrobenzoic acid) .2% triton X-100) and performed at 412 nm with 50mM oxaloacetate to start the reaction. Readings were obtained for 5 minutes at 30°C. Normalization was again to protein concentration.

Real-time PCR

Maxima SYBR Green/ROX qPCR master mix (Fermentas) was used according to manufacturer's directions to perform real time PCR. Primers used for the cDNA quantification were: PGC-1α (5′CTGCGGGATGATGGAGACA, 5′ AGCAGCGAAAGCGTCACA), PGC-1β (5′TGGCCCAGATACACTGACTATG, 5′TGGGCCTCTTTCAGTAAGCT), β-Actin (5′ TGACAGGATGCAGAAGGAGAT, 5′GCGCTCAGGAGGAGCAAT). The following primer pairs were used for the quantification of mtDNA copy number in total DNA (extracted with phenol: chloroform): ND1 (5′ CAGCCTGACCCATAGCCATA, 5′ ATTCTCCTTCTGTCAGGTCGAA), GADPH (5′ GCAGTGGCAAAGTGGAGATT, 5′ GAATTTGCCGTGAGTGGAGT). Comparative Ct method was used to determine the relative abundance of mtDNA or genes of interest (Schmittgen and Livak, 2008).

In situ COX Activity Histochemistry

Mice were transcardially perfused with ice cold PBS (pH 7.4) containing 4% paraformaldehyde (PFA) and 4% sucrose. Brains were quickly isolated and submerged in 4% paraformaldehyde at 4 °C for 1 hour and then cryoprotected by increasing concentrations of sucrose solutions (10%, 20%, and then 30%) prepared in PBS. The cryoprotected brains were positioned in a plastic block (Polysciences), submerged in the OCT Compound solution (TissueTek) diluted with an equal volume of 25% sucrose, and quickly frozen by submerging the plastic block into 2-methylbutane cooled in liquid nitrogen. 20 μM thick sections were cut on a cryostat and warmed.

For neuroanatomical evaluation of brains, sections were stained with cresyl violet solution (0.1%) for 3 minutes, dehydrated with increasing concentrations of ethanol, and cleared with xylenes before mounting with Sub-X mounting medium (Surgipath). Images were captured with an Olympus Bx51 microscope at 4× or 60× magnification.

COX histochemistry was performed using 0.05% 3,3′-diaminobenzidine (DAB), 0.02% cytochrome *c*, and 4% sucrose for 3 hours in the dark at 37°C. After incubation, sections were washed with deionized water, dehydrated, cleared with xylenes, mounted, and imaged as described above.

RotaRod

Motor coordination was evaluated with the RotaRod equipment (IITC Life Sciences) designed for mice. Animals were tested on a monthly basis with four runs on a given day with two runs for practice. The final two runs were recorded and combined to find the

average latency to fall. A resting period of 45 minutes between each run was given. Animals were required to position limbs to stay on a rotating rod accelerating from 6 rpm-20 rpm over a 300 second time period. Mice that had completed the task received a final latency time of 300 seconds.

Radial 6-Arm Water Maze

Spatial memory behavioral test modified for mice was previously described (Rodenas-Ruano et al., 2006). Male animals were trained and tested over a one week period. The hidden platform remained stationary in one arm for the duration of the test. The starting arm releasing the animal was randomized. A 60 second maximum time allotment was given for animals to locate and swim to the platform. Mice who failed to find the platform were directed to it after the 60 seconds. A 30 second rest was given before the animal was again randomly placed in another arm. Data collection for wrong corridor selection and latency to reach the platform occurred on the fourth and fifth test days.

Magnetic Resonance Imaging

MRI data were obtained at the 4.7 Telsa Animal MRI Research Facilities at the Miller School of Medicine of the University of Miami.

Statistical Analysis for Behavior

Mito-PstI mice (PstI+/tTA+ , n=9) and their control counterparts (PstI+/tTA−, n=11) were weighed every two weeks and subjected to behavioral characterization. The comparison of weight data was performed using one-way ANOVA. Data from spatial memory and motor coordination tasks were analyzed using a two-tailed, unpaired Student *t* test. Differences were considered significant when $p < 0.05$.

Results

Characterization of neuronal expression of mito-PstI in transgenic mice

Mito-PstI mice had the expression of mito-PstI regulated by a minimal promoter containing a tetracycline response element (TRE) (Fukui and Moraes, 2009). We mated these Mito-PstI + transgenic mice with mice expressing tetracycline transactivator (tTA) protein under the control of CamKIIα promoter (tTA+ mice). Subsequent matings produced male animals that were positive for both alleles (mito-PstI+/tTA+) (Figure 1A). For simplicity, we refer to these double transgenic mice as “Mito-PstI mice”. In this tet-off system, in the absence of doxycycline, tTA protein expressed under the CamKIIα promoter binds to TRE and induces the expression of mito-PstI. Male siblings, which are positive for either allele (mito-PstI+/tTA− or mito-PstI−/tTA+), do not express mito-PstI protein and therefore were used as controls. The transgenic line used in this study (Line 5752) differed from the line described in our previous report (Line 5751); Although the mito-PstI was expressed in the same region-specific manner in both lines, Line 5752 expresses approximately 15-fold lower levels of mito-PstI protein than Line 5751 (Fukui and Moraes, 2009). Animals (tet-off) were continuously induced from birth and kept on the standard rodent diet. The *Pst*I restriction sites on the mtDNA reside at nucleotide (nt) positions 8,420 and 12,238 (Figure 1B).

Before comparing differences in regional vulnerability in the Mito-PstI model, we first determined whether there was a regional difference in the expression of mito-PstI protein. Using western blot analysis, we detected mito-PstI protein in the cortex, hippocampus, and striatum but very little in the cerebellum (Figure 1C). Expression was absent in controls. We also observed no significant differences in the steady-state levels of mito-PstI when quantified and compared across regions (Figure 1D).

Expression of mito-PstI in forebrain neurons leads to a progressive neurodegenerative phenotype

At birth, animals from all genotypes appeared normal and litters showed expected Mendelian ratios. Mito-PstI animals began showing slower weight gain at 2 months with an obvious smaller appearance at 10-14 months as compared to control animals (Figure 2A). There were no differences in lifespan up to 16 months of age. At 16 months, the remaining Mito-PstI and controls of this group were sacrificed for biochemical analysis.

Mito-PstI mice presented no overt phenotypic abnormalities until 6-8 months. At this time Mito-PstI animals displayed an abnormal limb clasping phenotype during a gravitational tail hang (Figure 2C). Control animals displayed a normal escape response when hung upside-down where the limbs were extended outwards for protection from threat of a fall. Although the neural basis of this abnormal phenotype has not been elucidated, it has been reported in other mouse models that exhibit striatum degeneration (Hara et al., 2006; Komatsu et al., 2006).

Due to this limb clasping phenotype, we tested Mito-PstI mice at 3, 5 and 11 months-of-age for their ability to coordinate limb positioning on the RotaRod. Mito-PstI and control mice performed with equal abilities at the 3 month time point; however, Mito-PstI animals performed progressively worse in their ability to stay on the rotating rod at the 5 and 11 month time point (Figure 2B). These findings of restricted weight gain, abnormal clasping, and poor motor skill performance suggested that Mito-PstI animals had a progressive age-related neurodegeneration of the locomotive centers of the brain.

Because mito-PstI expression was also observed in the hippocampus, we tested 14-month old Mito-PstI mice for their spatial memory and learning abilities in a radial water maze paradigm. Mice expressing mito-PstI performed poorly when compared to age-matched controls. The time to find the hidden platform was approximately 4 times longer for the Mito-PstI mice, and Mito-PstI mice committed significantly more errors in choosing the correct arm ($p<0.001$, not shown).

Mito-PstI expression causes massive neurodegeneration of the striatum and cortical atrophy

These behavioral phenotypes suggested the Mito-PstI mice had progressive neurodegenerative events occurring in the central nervous system (CNS), most prominently affecting neuroanatomical regions that control movement.

We began analysis at 2 months of age, prior to the motor phenotypes. There appeared to be no disturbances in the cortex and hippocampus at this time point. Brain from young 2 month-old Mito-PstI animals had normal gross morphology and neuroanatomy of these areas; however, in sagittal sections striatal tissue appeared less dense (Figure 3A).

We then analyzed various phenotypes from the time when the limb clasping phenotype was first observed. To better determine the general brain morphology *in vivo* during this degenerative process, Mito-PstI and control animals underwent MRI imaging at 6-8 months-of-age. Scans revealed that Mito-PstI animals' striatum had atrophied and to a lesser extent also the cortex that were replaced by fluid, likely cerebral spinal fluid (CSF) (Figure 3B). The widening of the lateral ventricles completely replaced areas of the dorsal striatum and ablated the shape of the striatum in ventral aspects. These CNS changes appeared even less severe in the hippocampus at this time point (Figure 3B). Gross brain anatomy was altered with a visible atrophy of the cortex and decrease in brain weight and size (Figure 3C).

This degeneration proved to be progressive as it worsened in Mito-PstI animals sacrificed at 14 months-of age. Histological analysis with cresyl violet revealed that Mito-PstI brains at both of these age groups had shrinkage of the cortical layer, hippocampus, and complete absence of the ventral striatum/amygdala region (Figure 3D). As previously mentioned, the dorsal striatum was completely absent. These results confirmed the suspected progressive neurodegeneration of the regions expressing mito-PstI. They also revealed that the striatum was more severely affected among other brain regions and was disrupted earlier in this neuronal OXPHOS-deficiency model.

Mito-PstI expression causes a depletion of mtDNA leading to an OXPHOS deficiency

The expression of mito-PstI leads to double-strand breaks in the mtDNA disrupting the synthesis of mtDNA-encoded proteins for OXPHOS (Srivastava and Moraes, 2005; Fukui and Moraes, 2009). To measure the extent of mtDNA depletion in the different neuroanatomical regions, we tested animals at 2 months-of-age, before the neurodegeneration became too severe to adequately assess mito-PstI induced changes in the striatum. We observed a significant ~30% depletion of mtDNA in the cerebral cortex and a ~40% decrease in the hippocampus and striatum in Mito-PstI mice at this age (Figure 4A). There were no significant changes in the levels of mtDNA in the cerebellum of Mito-PstI mice.

To determine the impact that this mtDNA depletion on OXPHOS function, we performed spectrophotometric enzymatic assays assessing the activity of cytochrome *c* oxidase (COX) (also called complex IV). MtDNA encodes 3 subunits of COX (Anderson et al., 1981). Therefore, we reasoned that the activity of this enzyme complex would be affected due to the reduction of mtDNA. Citrate synthase (CS) is an enzyme in the citric acid cycle, and its activity is not reduced by a reduction in OXPHOS. Therefore, the activity of this enzyme is related to the amount of mitochondria in each homogenate preparation and COX/CS can give a better estimate of COX activity per mitochondrial mass (Wiegand and Remington, 1986). At 2 months, there was a 40% decrease in the COX/CS ratio in the cortex, hippocampus and a 50% decrease in the striatum of Mito-PstI mice compared to controls (Figure 4B). *In situ* COX enzymatic activities showed a defect in cerebral cortex, hippocampus, and striatum confirming spectrophotometer results (not shown).

We performed western blots to determine the steady state levels of representative subunits of the different OXPHOS complexes. In the striatum, we detected significant decreases in protein levels for subunits of complexes I, II, and IV (Figure 4C-D). Decreases in COXI, a subunit of complex IV coded by mtDNA was observed in cortex , hippocampus, and cerebellum. However, there was a significant increase in SDHB in the hippocampus (Figure 4 C-D). No major changes in the other OXPHOS subunits tested were detected in these three regions (Figure 4C-D). These results suggest that multiple OXPHOS complexes containing mtDNA-encoded subunits were affected in striatum, whereas in the other brain regions we could detect a decrease only in the complex IV subunit, with a possible compensatory increase of mitochondrial levels in hippocampus.

Determining the Approximate Cell Population Makeup in Different Neuroanatomical Regions

Although the mito-PstI transgene is only expressed in neurons, the neuroanatomical regions of interest are made up of other non-neuronal cell types, the majority of which being astrocytes. We wanted to determine the relative profile of the homogenate cell pools we were analyzing.

We performed western blot analysis using Abs against β-III tubulin (a neuronal-specific cytoskeletal protein) and glial fibrillary acidic protein, GFAP (an astrocytic cytoskeletal protein) as markers to determine whether the ratios of neuronal or astrocytic-immunopositive cells were grossly altered in 6-month old Mito-PstI animals. Striatum had a higher relative β-III tubulin signal compared to cortex (Figure 5B-D). These results suggest that there are more neuronal processes/cell bodies in the striatum than in homogenates from the other two regions. The GFAP signals from all the brain regions were not markedly different; however, animals that expressed mito-PstI had an increase in GFAP signal, suggestive of astrogliosis (Figure 5A,C-D).

Mitochondrial Bioenergetics are Relatively Higher in the Striatum of Wild-Type Mice

After excluding the possibilities that there could be preferential mito-PstI expression or selective impairment of OXPHOS activity in the striatum, we began to explore the reason for an increased reliance on mitochondrial OXPHOS function in the striatal area. When measuring COX and CS activities in wild-type mice, we observed that different brain regions exhibit distinct activities of COX and CS (Figure 6A). It appeared that, in wild-type mice, striatum and cerebellum had both higher OXPHOS activity (inferred from the COX activity) and higher mitochondrial mass (assessed by CS activity) when compared to hippocampus and cerebral cortex.

PGC1-α and β have been shown to control mitochondrial levels, density and function in neurons (Wareski et al., 2009). Quantification of PGC-1β levels in different brain regions showed that striatum and cerebellum had relatively high PGC-1β levels (Figure 6B). PGC-1β and PGC-1α had similar expression patterns (Figure 6C).

To determine whether there were differences in basal levels of mitochondrial membrane potential (ΔΨm) across regions, we isolated and analyzed mitochondria from different brain regions of wild-type mice by TMRE-FACS. We observed a significantly higher ΔΨm in striatal-derived mitochondria when compared to cortical-derived mitochondria (Figure 6D). These results suggest that not all regions of the brain have the same mitochondrial physiology. The differential expression of PGC-1 transcription co-activators in different brain regions may explain such regional differences in the property of mitochondria, especially in the striatum.

Striatal Mitochondria is More Sensitive to Calcium

We wanted to determine whether the striatum mitochondria were more sensitive to a calcium stimulus as previously reported (Brustovetsky et al., 2003). In the cortex and hippocampus, a relatively low concentration of calcium increased the TMRE fluorescence (Figure 7A, B, E). In contrast, the calcium stimulus reduced the ΔΨm in the striatum (Figure 7C, E). There were no changes elicited in the cerebellum (Figure 7D, E).

Membrane Potential and Calcium Sensitivity are Preferentially Impaired in the Striatum of Mito-PstI mice

We also compared the ΔΨm between 2 month-old control and Mito-PstI animals across different brain regions. Although the ΔΨm was reduced in all brain regions expressing mito-PstI, it was significantly worse in the striatum (Figure 8A-D). We also wanted to determine whether the mito-PstI striatal mitochondria that retained high ΔΨm were still very sensitive to calcium. We observed that the Ca^{++} stimulus had no effect on cortical or even a slight stimulatory effect on hippocampal Mito-PstI mitochondria, but it further reduced the TMRE fluorescence of the mitochondria from the Mito-PstI striatum (Figure 8E). This suggests that the ΔΨm of Mito-PstI striatal mitochondria was more sensitive to disruptions than the ones in cortical and hippocampal regions.

Discussion

We report a mouse model with an OXPHOS dysfunction-associated progressive neurodegenerative phenotype characterized by vulnerability of the striatum. To our knowledge, such differences in mitochondrial function and response to dysfunction in distinct neuroanatomical regions *in vivo* have not been previously described. We compared cortex, hippocampus, and striatum with a similar insult, namely, mtDNA damage by mito-PstI expression. All regions with mito-PstI expression were affected with progressive neurodegenerative pathology. However, the striatum was particularly susceptible with an almost complete ablation of this neuroanatomical region. Because the striatum is rich in neuronal projections, soma counting cannot fully reflect the loss of neurons. However, the higher susceptibility of striatum neurons is also reflected by the fact that mito-PstI positive neurons still exist in cortex and hippocampal samples at 14 months-of-age (data not shown) at a time point when striatum can no longer be harvested due to its ablation. Nonetheless, the cellular heterogeneity of homogenates does provide a limitation, which should be taken into consideration when interpreting the results.

We did not observe this preferential susceptibility in a previously reported transgenic line expressing higher levels of mito-PstI (line 5751). In that model, the CamKIIα-driven expression of mito-PstI caused an acute and massive depletion of mtDNA leading to premature death at 3-4 months-of-age (Fukui and Moraes, 2009). In this high mito-PstI expression model (15-fold higher than the model described here), we still see a widening of the lateral ventricles and degeneration of the striatum (data not shown); however, it is likely that the speed of degeneration did not allow us to notice that the striatum was both first affected and completely ablated before death.

Previous publications have also suggested regional and neuronal differences in susceptibility to OXPHOS deficiency. PGC1-α null mice had regional-specific spongiform neurodegeneration occurring in the striatum and to a lesser extent the cortex and hippocampus even though the absence of the gene was ubiquitous (Lin et al., 2004; Leone et al., 2005). PGC1-α expression occurs in the cerebral cortex, hippocampus, cerebellum, striatum, and thalamus, particularly in GABAergic neuronal subtypes (Cowell et al., 2007). This subtype of neurons is enriched in the striatum as medium spiny neurons. In Huntington's disease, mutant huntingtin has been shown to transcriptionally repress PGC-1α leading to mitochondrial dysfunction by interfering with cAMP responsive element binding protein (CREB) (Cui et al., 2006). CREB conditional knockouts targeted to CAMKIIα-expressing neurons also show massive degeneration and atrophy of the striatum and CA1 region of the hippocampus, resembling the degeneration patterns seen in the PGC-1α null mice (Mantamadiotis et al., 2002). Our model also parallels this type of striatal degeneration, with cortex and hippocampus being affected later in the disease process. A report of another genetically manipulated model of mitochondria OXPHOS dysfunction (neuronal-specific transcription factor A [TFAM] null mouse) did not describe a preferential striatal defect. However, there was substantial degeneration of the striatum, in addition to the ones observed in the neocortex and hippocampus (Sorensen et al., 2001; Dufour et al., 2008). Most recently, a study looking at the genetic and siRNA ablation of Coenzyme Q in *C.Elegans* noted a particular and specific vulnerability and degeneration of only GABAergic, neurons (Earls et al. 2010).

Due to the non-homogenous cell populations in brain, *in vivo* results can be difficult to interpret. A non-homogenous cell population in the brain can mask OXPHOS deficits and mtDNA quantities as not all cell types express mito-PstI, potentially leading to an underestimation of the defects in neurons. Although western blots showed that striatum does have relatively higher levels of the neuronal marker βIII tubulin, we detected comparable

levels of mito-PstI expression, mtDNA depletion and COX deficiency in cortex, hippocampus and striatum in two month-old Mito-PstI mice. Therefore, it appears that under chronic OXPHOS deficiencies striatal neurons are more sensitive than hippocampal or cortical neurons.

Why do different brain regions have different susceptibility to OXPHOS defects? We envision at least two possibilities: 1) OXPHOS enzymes in the striatum are more sensitive to the reduction in mtDNA coded subunits. Curiously, complex II subunits were also decreased in the striatum, and we do not have an explanation for this observation. 2) We showed that wild-type cortex, hippocampus, striatum, and cerebellum have differences in mitochondrial enzymes activity and $\Delta\Psi m$, with striatum showing relatively higher levels of these markers. These differences may be related to the cellular composition, but may be also related to the higher PGC-1α and β expression in the striatum. This increased dependence on OXPHOS, perhaps to maintain a high $\Delta\Psi m$ (see below), could make the striatum more sensitive to partial defects.

Other studies have also shown that mitochondria from different regions react differently to calcium stress. Studies using primary cultures showed an increased vulnerability of striatal-derived neurons and astrocytes to calcium when comparing to cells derived from the cerebral cortex (Oliveira and Goncalves, 2009). Work from Dubinsky's group found that striatal mitochondria isolated from rats were more sensitive than cortical mitochondria in their response to calcium perhaps due to increased amounts of cyclophilin D, a mitochondrial permeability transition pore component (Brustovetsky et al., 2003; LaFrance et al., 2005). Our study also showed a depolarization of $\Delta\Psi m$ when striatal mitochondria from wild-type and Mito-PstI animals are treated with low calcium levels. This calcium concentration did not promote a collapse in $\Delta\Psi m$ in cortical and hippocampal mitochondria, but rather increased $\Delta\Psi m$, probably because of an activation of mitochondrial dehydrogenases (Brookes et al., 2004).

We also found significant astrogliosis in the cortex and hippocampus but not in the striatum of Mito-PstI mice. This finding raises the possibility that astrocytes may provide bioenergetic support to OXPHOS-disrupted neurons (Kasischke et al., 2004).

We propose the following model to explain the relatively high striatal susceptibility to an OXPHOS defect (Figure 9). The striatum mitochondria have intrinsically higher OXPHOS function, and a higher basal $\Delta\Psi m$, which is prone to collapse when OXPHOS activity is reduced. Because the rate of Ca^{++} uptake depends on a robust proton motive force, we propose that under these conditions of low OXPHOS, cytosolic Ca^{++} levels would increase, leading to cell death. The mitochondrial permeability transition does not need to be evoked, although it may be involved as the striatum $\Delta\Psi m$ is very sensitive to Ca^{++} as well. In either case, toxic levels of Ca^{++} would accumulate preferentially in the cytosol of striatal neurons.

In summary, we have created a novel mouse model of mtDNA depletion by expressing relatively low levels of mito-PstI in CNS neurons, which leads to a chronic OXPHOS deficiency. This mouse model develops a progressive neurodegenerative phenotype with a preferential degeneration of the striatum. These results shed new light into how mitochondria contribute to regional differences in neurodegenerative pathologies such as in Huntington's disease and stroke.

Acknowledgments

This work was supported in part by the National Institutes of Health Grants 1R01AG036871, 5R56NS041777 (C.T.M), 5T32NS007492, 5T32NS007459, Lois Pope LIFE Fellowship (A.M.P.). We thank Dr. John Barrett

(University of Miami) for critically reading the manuscript, Dr. Kyle Padgett for the MRI images and the Flow Cytometry Core at the UM Sylvester Comprehensive Cancer Center for assistance.

References

Anderson S, Bankier AT, Barrell BG, de Bruijn MH, Coulson AR, Drouin J, Eperon IC, Nierlich DP, Roe BA, Sanger F, Schreier PH, Smith AJ, Staden R, Young IG. Sequence and organization of the human mitochondrial genome. Nature. 1981; 290:457–465. [PubMed: 7219534]

Barrientos A. In vivo and in organello assessment of OXPHOS activities. Methods. 2002; 26:307–316. [PubMed: 12054921]

Berthet C, Lei H, Thevenet J, Gruetter R, Magistretti PJ, Hirt L. Neuroprotective role of lactate after cerebral ischemia. J Cereb Blood Flow Metab. 2009; 29:1780–1789. [PubMed: 19675565]

Betarbet R, Sherer TB, MacKenzie G, Garcia-Osuna M, Panov AV, Greenamyre JT. Chronic systemic pesticide exposure reproduces features of Parkinson's disease. Nat Neurosci. 2000; 3:1301–1306. [PubMed: 11100151]

Brookes PS, Yoon Y, Robotham JL, Anders MW, Sheu SS. Calcium, ATP, and ROS: a mitochondrial love-hate triangle. Am J Physiol Cell Physiol. 2004; 287:C817–833. [PubMed: 15355853]

Brustovetsky N, Brustovetsky T, Purl KJ, Capano M, Crompton M, Dubinsky JM. Increased susceptibility of striatal mitochondria to calcium-induced permeability transition. J Neurosci. 2003; 23:4858–4867. [PubMed: 12832508]

Cowell RM, Blake KR, Russell JW. Localization of the transcriptional coactivator PGC-1alpha to GABAergic neurons during maturation of the rat brain. J Comp Neurol. 2007; 502:1–18. [PubMed: 17335037]

Cui L, Jeong H, Borovecki F, Parkhurst CN, Tanese N, Krainc D. Transcriptional repression of PGC-1alpha by mutant huntingtin leads to mitochondrial dysfunction and neurodegeneration. Cell. 2006; 127:59–69. [PubMed: 17018277]

Dufour E, Terzioglu M, Sterky FH, Sorensen L, Galter D, Olson L, Wilbertz J, Larsson NG. Age-associated mosaic respiratory chain deficiency causes trans-neuronal degeneration. Hum Mol Genet. 2008; 17:1418–1426. [PubMed: 18245781]

Earls LR, Hacker ML, Watson JD, Miller DM. Coenzyme Q protects Caenorhabditis elegans GABA neurons from calcium-dependent degeneration. PNAS. 2010; 107:14460–5. [PubMed: 20663955]

Fukui H, Moraes CT. Extended polyglutamine repeats trigger a feedback loop involving the mitochondrial complex III, the proteasome and huntingtin aggregates. Hum Mol Genet. 2007; 16:783–797. [PubMed: 17356014]

Fukui H, Moraes CT. Mechanisms of formation and accumulation of mitochondrial DNA deletions in aging neurons. Hum Mol Genet. 2009; 18:1028–1036. [PubMed: 19095717]

Guyot MC, Hantraye P, Dolan R, Palfi S, Maziere M, Brouillet E. Quantifiable bradykinesia, gait abnormalities and Huntington's disease-like striatal lesions in rats chronically treated with 3-nitropropionic acid. Neuroscience. 1997; 79:45–56. [PubMed: 9178864]

Hara T, Nakamura K, Matsui M, Yamamoto A, Nakahara Y, Suzuki-Migishima R, Yokoyama M, Mishima K, Saito I, Okano H, Mizushima N. Suppression of basal autophagy in neural cells causes neurodegenerative disease in mice. Nature. 2006; 441:885–889. [PubMed: 16625204]

Kasischke KA, Vishwasrao HD, Fisher PJ, Zipfel WR, Webb WW. Neural activity triggers neuronal oxidative metabolism followed by astrocytic glycolysis. Science. 2004; 305:99–103. [PubMed: 15232110]

Kirkinezos IG, Bacman SR, Hernandez D, Oca-Cossio J, Arias LJ, Perez-Pinzon MA, Bradley WG, Moraes CT. Cytochrome c association with the inner mitochondrial membrane is impaired in the CNS of G93A-SOD1 mice. J Neurosci. 2005; 25:164–172. [PubMed: 15634778]

Komatsu M, Waguri S, Chiba T, Murata S, Iwata J, Tanida I, Ueno T, Koike M, Uchiyama Y, Kominami E, Tanaka K. Loss of autophagy in the central nervous system causes neurodegeneration in mice. Nature. 2006; 441:880–884. [PubMed: 16625205]

LaFrance R, Brustovetsky N, Sherburne C, Delong D, Dubinsky JM. Age-related changes in regional brain mitochondria from Fischer 344 rats. Aging Cell. 2005; 4:139–145. [PubMed: 15924570]

Lee DR, Helps SC, Macardle PJ, Nilsson M, Sims NR. Alterations in membrane potential in mitochondria isolated from brain subregions during focal cerebral ischemia and early reperfusion: evaluation using flow cytometry. Neurochem Res. 2009; 34:1857–1866. [PubMed: 19488856]

Leone TC, Lehman JJ, Finck BN, Schaeffer PJ, Wende AR, Boudina S, Courtois M, Wozniak DF, Sambandam N, Bernal-Mizrachi C, Chen Z, Holloszy JO, Medeiros DM, Schmidt RE, Saffitz JE, Abel ED, Semenkovich CF, Kelly DP. PGC-1alpha deficiency causes multi-system energy metabolic derangements: muscle dysfunction, abnormal weight control and hepatic steatosis. PLoS Biol. 2005; 3:e101. [PubMed: 15760270]

Lin J, Wu PH, Tarr PT, Lindenberg KS, St-Pierre J, Zhang CY, Mootha VK, Jager S, Vianna CR, Reznick RM, Cui L, Manieri M, Donovan MX, Wu Z, Cooper MP, Fan MC, Rohas LM, Zavacki AM, Cinti S, Shulman GI, Lowell BB, Krainc D, Spiegelman BM. Defects in adaptive energy metabolism with CNS-linked hyperactivity in PGC-1alpha null mice. Cell. 2004; 119:121–135. [PubMed: 15454086]

Lin MT, Beal MF. Mitochondrial dysfunction and oxidative stress in neurodegenerative diseases. Nature. 2006; 443:787–795. [PubMed: 17051205]

Mantamadiotis T, Lemberger T, Bleckmann SC, Kern H, Kretz O, Villalba A Martin, Tronche F, Kellendonk C, Gau D, Kapfhammer J, Otto C, Schmid W, Schutz G. Disruption of CREB function in brain leads to neurodegeneration. Nat Genet. 2002; 31:47–54. [PubMed: 11967539]

Mattson MP, Gleichmann M, Cheng A. Mitochondria in neuroplasticity and neurological disorders. Neuron. 2008; 60:748–766. [PubMed: 19081372]

Oliveira JM, Goncalves J. In situ mitochondrial Ca2+ buffering differences of intact neurons and astrocytes from cortex and striatum. J Biol Chem. 2009; 284:5010–5020. [PubMed: 19106091]

Orr AL, Li S, Wang CE, Li H, Wang J, Rong J, Xu X, Mastroberardino PG, Greenamyre JT, Li XJ. N-terminal mutant huntingtin associates with mitochondria and impairs mitochondrial trafficking. J Neurosci. 2008; 28:2783–2792. [PubMed: 18337408]

Pickrell AM, Moraes CT. What role does mitochondrial stress play in neurodegenerative diseases? Methods Mol Biol. 648:63–78. [PubMed: 20700705]

Rodenas-Ruano A, Perez-Pinzon MA, Green EJ, Henkemeyer M, Liebl DJ. Distinct roles for ephrinB3 in the formation and function of hippocampal synapses. Dev Biol. 2006; 292:34–45. [PubMed: 16466709]

Schmittgen TD, Livak KJ. Analyzing real-time PCR data by the comparative C(T) method. Nat Protoc. 2008; 3:1101–1108. [PubMed: 18546601]

Schon EA, Manfredi G. Neuronal degeneration and mitochondrial dysfunction. J Clin Invest. 2003; 111:303–312. [PubMed: 12569152]

Sorensen L, Ekstrand M, Silva JP, Lindqvist E, Xu B, Rustin P, Olson L, Larsson NG. Late-onset corticohippocampal neurodepletion attributable to catastrophic failure of oxidative phosphorylation in MILON mice. J Neurosci. 2001; 21:8082–8090. [PubMed: 11588181]

Srivastava S, Moraes CT. Double-strand breaks of mouse muscle mtDNA promote large deletions similar to multiple mtDNA deletions in humans. Hum Mol Genet. 2005; 14:893–902. [PubMed: 15703189]

Wang H, Lim PJ, Karbowski M, Monteiro MJ. Effects of overexpression of huntingtin proteins on mitochondrial integrity. Hum Mol Genet. 2009; 18:737–752. [PubMed: 19039036]

Wareski P, Vaarmann A, Choubey V, Safiulina D, Liiv J, Kuum M, Kaasik A. PGC-1{alpha} and PGC-1{beta} regulate mitochondrial density in neurons. J Biol Chem. 2009; 284:21379–21385. [PubMed: 19542216]

Wiegand G, Remington SJ. Citrate synthase: structure, control, and mechanism. Annu Rev Biophys Biophys Chem. 1986; 15:97–117. [PubMed: 3013232]

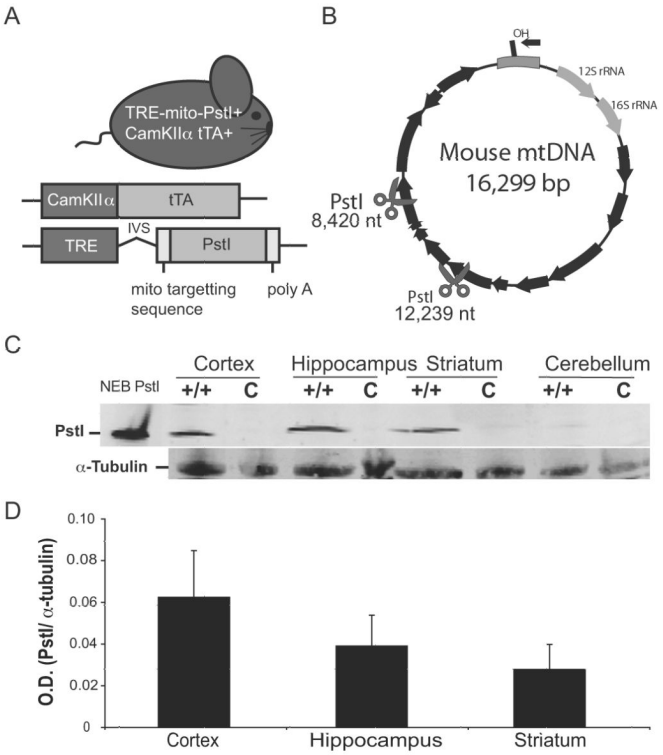

Figure 1. Mito-PstI mouse expresses mitochondrial-targeted restriction endonuclease in the central nervous system

A, Schematic representation of the experimental mito-PstI mouse and the transgenic constructs it harbors. ***B,*** Representative mtDNA map showing the targeted sites of *Pst*I at 8,420 and 12, 239 nt (scissors). Black arrows denote protein-coding genes. ***C,*** Western blots of brain lysates using antibodies probing for mito-PstI protein expressed in four regions of the CNS, cortex, hippocampus, striatum, and cerebellum 2 months-old mito-PstI (+/+) or control (c) animals. α-tubulin immunoreactivity was used to ensure equal protein loading. ***D,*** Quantification of the optical density (O.D.) of immunoblotted PstI protein levels from mito-PstI mice. Results are normalized against α-tubulin immunoreactivity. Values are mean ± SEM (n=3, p= NS).

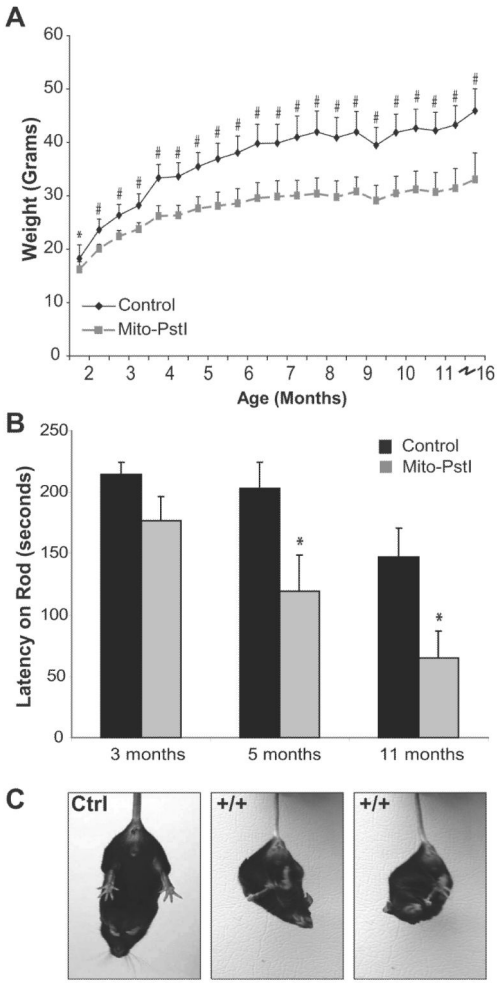

Figure 2. Mito-PstI mice displayed abnormal motor behaviors indicative of a progressive neurodegenerative pathology

A, Mito-PstI mice had significantly less body weight than controls. By the end of the study, Mito-PstI animals were approximately half the weight of controls. ***B,*** RotaRod behavioral testing revealed that Mito-PstI mice showed deficits on the ability to coordinate movement and balance on a rotating rod. Mito-PstI mice had shorter latency times when testing as compared to controls at 5 and 11 month time points. ***C,*** Mito-PstI mice display an abnormal clasping phenotype during a gravitational tail hang. Controls showed a proper limb extension behavior for escape. Phenotype appears around 6-7 months of age and persists for the rest of life. Values are mean ± SEM (control n=11, mito-PstI=9, * $p < 0.05$, #<0.001).

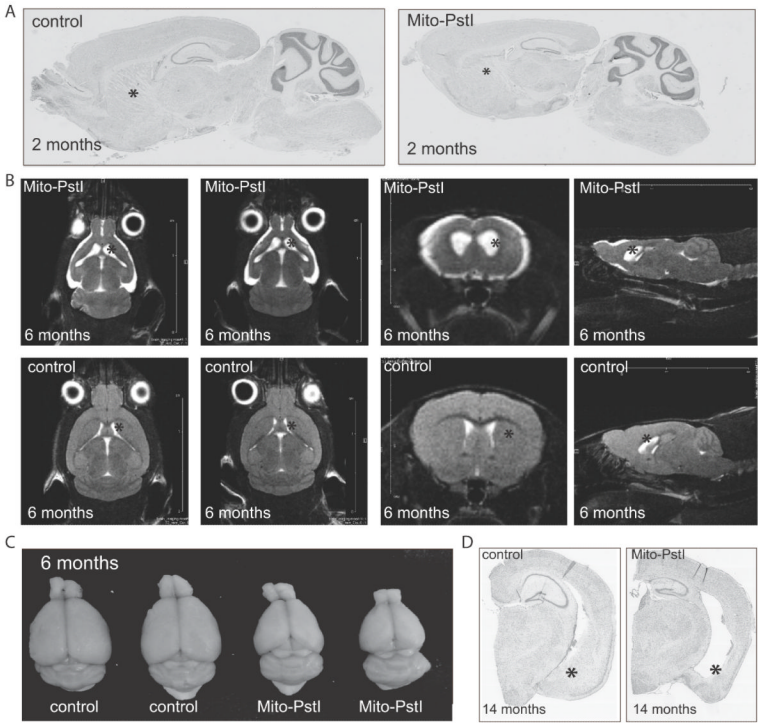

Figure 3. Mito-PstI mice have an age-related neurodegeneration with a preferential degeneration of the striatum

A, Parasagittal Nissl stained histological sections of 2-month old animals. ***B,*** Nuclear magnetic resonance imaging of 6-7-month old control and mito-PstI mice *in vivo* reveal ongoing degeneration with ablation of the striatum with cortical atrophy. Striatum denoted by asterisks. White areas represent cerebral spinal fluid. (n=2/group). ***C,*** Gross morphology reveals abnormal brain size and appearance of mito-PstI animals as compared to control at 6-7 months of age. Control brain weight ~0.42-0.45 g to mito-PstI weight ~0.27-0.30 g. ***D,*** Nissl-staining of coronal sections reveals that, at 14 months of age, degeneration occurs in the ventral aspects of the striatum denoted by asterisks that in absent in controls. Asterisk marks the striatum.

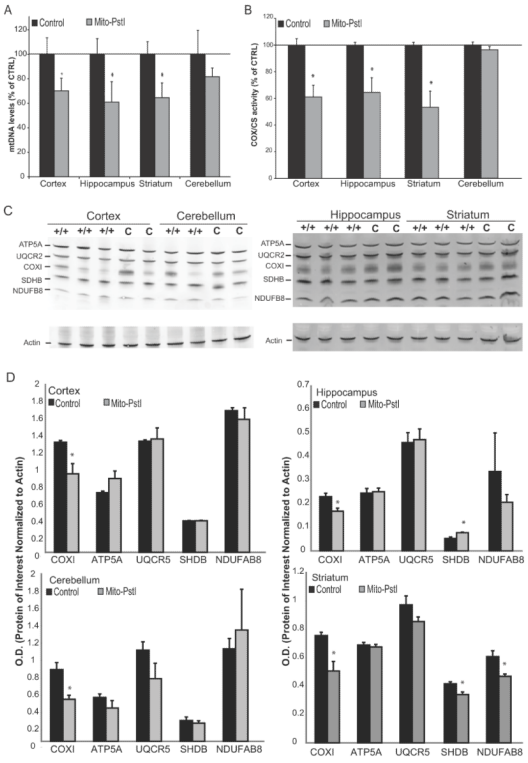

Figure 4. Mito-PstI expression causes an mtDNA depletion that leads to an OXPHOS deficiency

A, Real-time PCR measuring the levels of mtDNA against the nuclear gene GADPH. Isolated DNA was extracted from cortex, hippocampus, striatum, and cerebellum from 2-month old control and Mito-PstI animals and used as the template. Values are mean ± SEM (n=4-5/group, * p<0.05). Each sample was run in triplicate. ***B,*** Ratios of enzymatic COX activity to CS activity comparing control and Mito-PstI animals in different CNS regions at 2 months-of-age. Values are mean ± SEM (n=4-5/group, * p<.05,). Results are shown as a percentage of the control. ***C.*** Representative western blot analyses showing OXPHOS protein subunits from cortical, hippocampal, cerebellar, and striatal lysates: Complex V ATPase subunit α (ATP5A), Complex III Core 2 (UQCR2), Complex IV (COXI), Complex II subunit 30kDa (SDHB),Complex I (NDUFB8) between 2 month control (C) and Mito-PstI (+/+) animals (n=2-3/group). Actin immunoreactivity was used as a control to ensure equal protein loading. ***D,*** Optical density measurements of the protein of interest normalized to the signal from actin between 2 month control (C) and Mito-PstI (+/+) animals (n=3/group) * = p<.05.

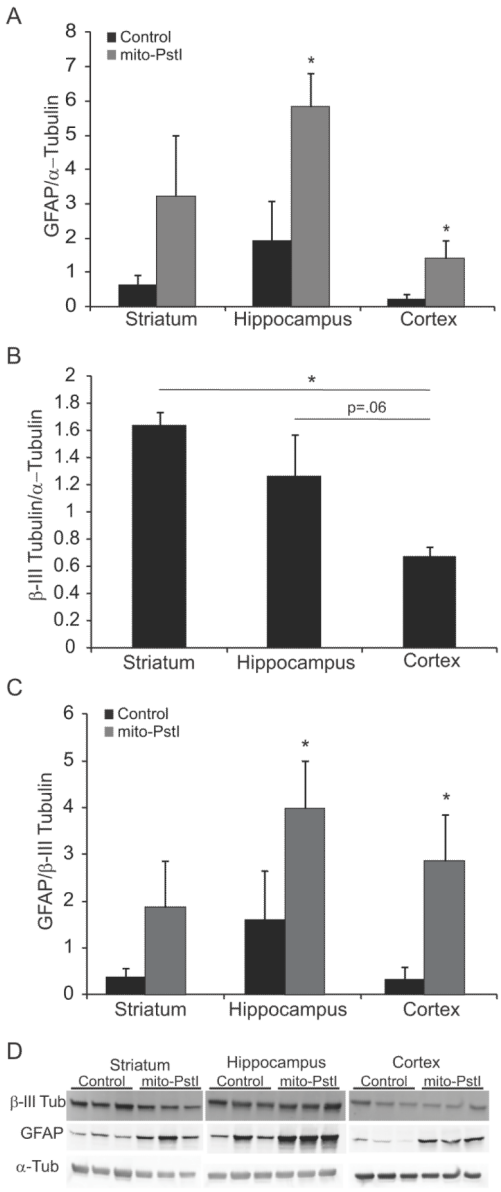

Figure 5. Striatum is enriched in neuronal-derived cells

A, Ratio of the optical density of immunoreactive GFAP/α-tubulin from a western blots of striatal, cortical and hippocampal homogenates from 6 month-old animals. ***B,*** Ratio of the optical density of immunoreactive β-III tubulin/α-tubulin of western blots of striatal, cortical and hippocampal homogenates from 6 month old animals.. ***C,*** Ratio of the optical density of immunoreactive GFAP/β-III tubulin western blots of striatal, cortical and hippocampal homogenates from 6 month old animals. ***D,*** Western blots from where quantitations were performed. Error bars=S.D., *=p<0.5, n=3.

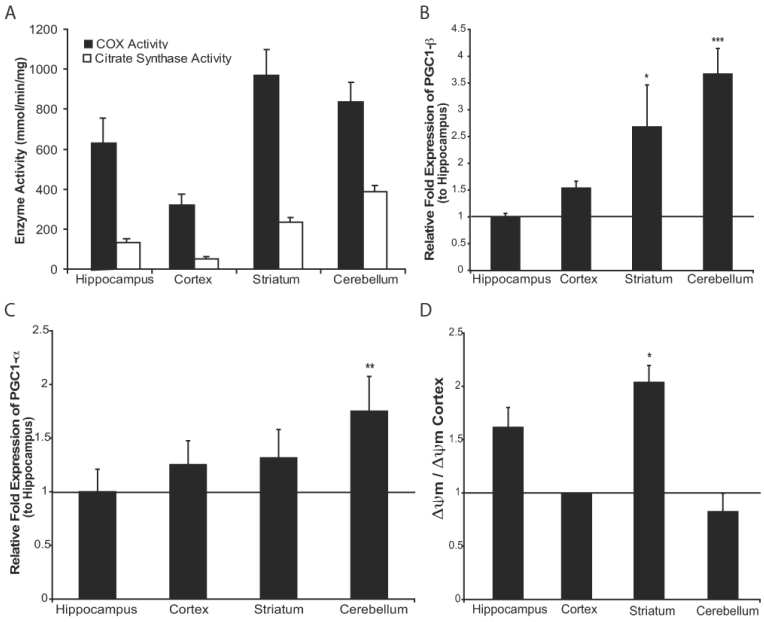

Figure 6. Striatum has a relatively high mitochondrial bioenergetics

A. COX activity and CS spectrophotometer assays comparing the activity per mg of protein in cortex, hippocampus, striatum, and cerebellum. Values are mean ± SEM (n=4-5/group). Significance between regional comparisons for COX activity (cortex v. hippocampus p=0.0015, hippocampus v. striatum p=0.013, striatum v. cortex p= 0.0012, cerebellum v. cortex p=0.041, cerebellum v. hippocampus p=NS, cerebellum v. striatum p=NS). Significance between regional comparisons for CS activity (cortex v. hippocampus p=0.0044, hippocampus v. striatum p=0.0017, striatum v. cortex p=0.00011, cerebellum v. cortex p=8.27E-.06, cerebellum v. hippocampus p=6.80E-.06, cerebellum v. striatum p=0.00049). ***C,*** Relative fold expression of PGC1-β levels compared to hippocampus when normalized to β-actin expression. Values are mean ± SEM (control n=4-5, mito-PstI=4-5, * p<0.05, **p<0.01 *** p < 0.001). *C.* Relative fold expression of PGC1-α levels compared to hippocampus when normalized to β-actin expression. Values are mean ± SEM (control n=4-5, mito-PstI=4-5, ** p < 0.01). ***D,*** Region-specific geometric mean of fluorescence of isolated mitochondria stained with TMRE. Values are mean ± SEM (control n=4-5, mito-PstI=4-5, * p<0.05).

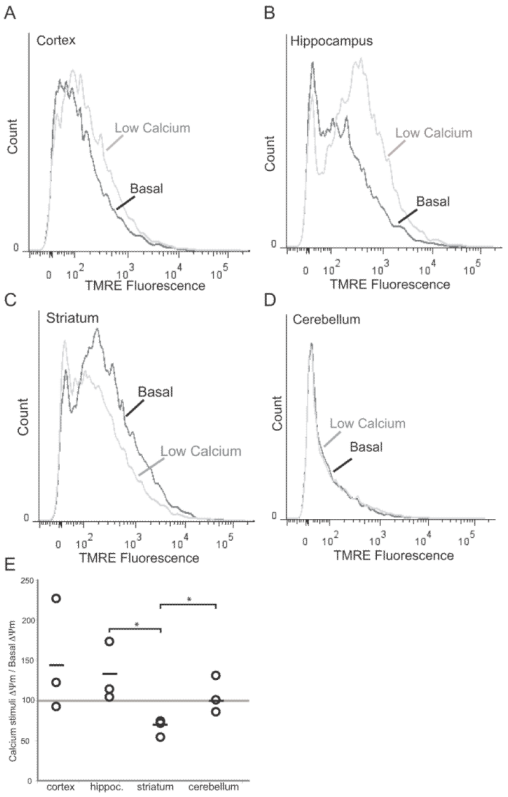

Figure 7. Mitochondrial membrane potential from striatum mitochondria of wild-type mice is highly sensitive to calcium stimulation

Histograms depicting TMRE fluorescence of mitochondria from a two month-old wild-type mouse at basal conditions or treated with calcium (0.3μmol/mg protein). A, cortex; B, hippocampus; C, striatum; D, cerebellum. ***E,*** Plotted changes in ($\Delta\Psi m[Ca^{++}]/\Delta\Psi m$ basal) from cortex, hippocampus, striatum, and cerebellum Circles represent individual animals (n=3). Horizontal line represents mean. (*$p < 0.05$).

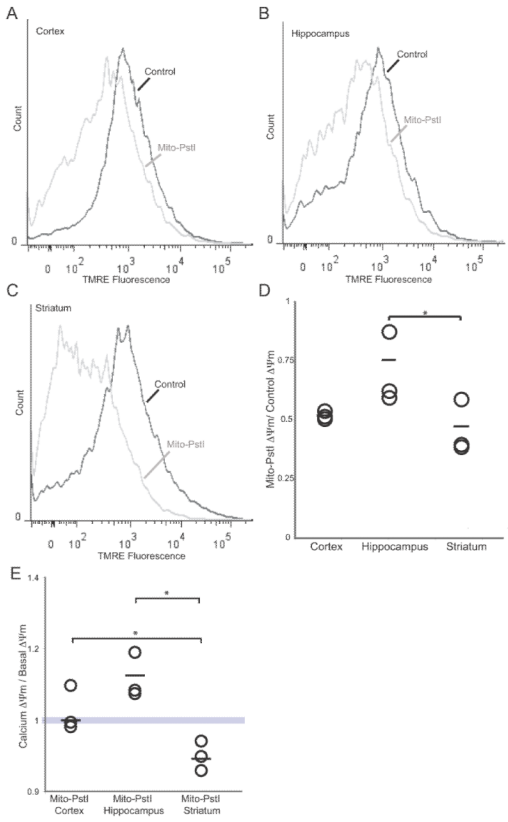

Figure 8. Basal ΔΨm is particularly decreased in the striatum of mito-PstI mice

Histograms depicting TMRE fluorescence of mitochondria from two month-old wild-type and Mito-PstI mice mouse at basal conditions. A, cortex. B, hippocampus. C, striatum. ***D,*** Plotted changes in Mito-PstI ΔΨm/wild-type ΔΨm of cortex, hippocampus, and striatum. Circles represent individual animals (n=3). Horizontal line represents mean. (*$p < 0.05$). ***E***, Plotted changes of the ratio of ΔΨm of cells treated with low calcium to basal ΔΨm of the cortex, hippocampus, and striatum of Mito-PstI animals. Geometric fluorescence values were determined when gating for high ΔΨm mitochondria. Circles represent individual animals (n=3). Horizontal line represents mean. (*$p < 0.05$).

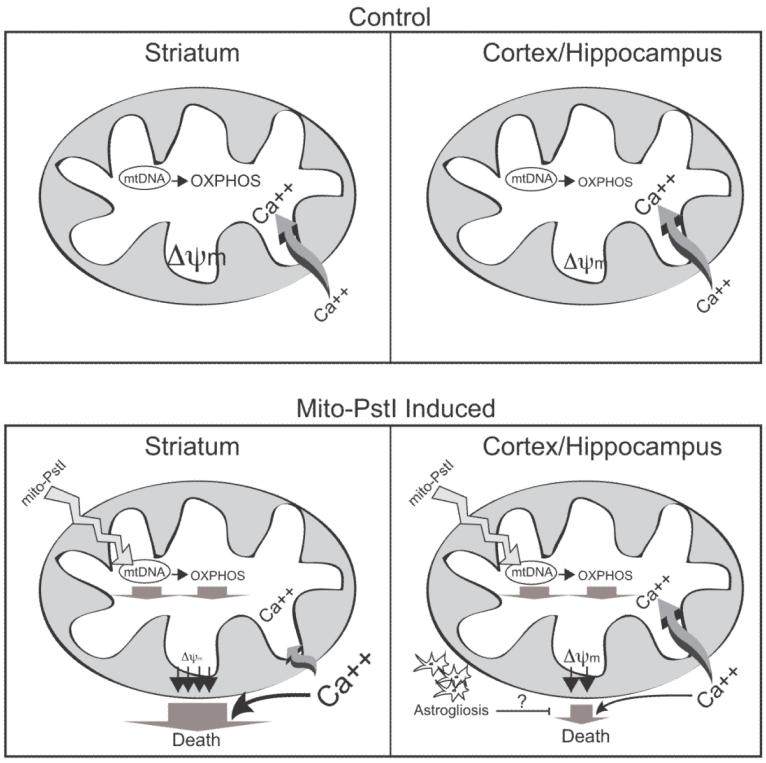

Figure 9. Proposed mechanism for the striatum vulnerability to OXPHOS defects

The upper panels depict a model under normal conditions. Control striatal mitochondria would have robust OXPHOS function, membrane potential, and would be more sensitive to a calcium stimulus as compared to cortical/hippocampal mitochondria. The lower panels depict the consequences of mito-PstI expression. Mito-PstI leads to mtDNA damage and decreases in OXPHOS. OXPHOS-dependent ΔΨm is relatively high in the striatum, and the OXPHOS defect leads to a marked collapse in ΔΨm with a consequent impairment in Ca^{++} buffering. This leads to increased cytosolic Ca^{++}, which activates Ca^{++}-sensitive proteases causing neuronal death. Astrocytosis, observed mostly in cortex and hippocampus after mito-PstI expression, may have a protective effect by supplying neurons with metabolic substrates (e.g. lactate) or other pro-survival factors.